HHS Public Access

Author manuscript

J Comp Neurol. Author manuscript; available in PMC 2016 May 01.

Published in final edited form as:

J Comp Neurol. 2015 May 1; 523(7): 1054–1072. doi:10.1002/cne.23707.

Stereological study of pyramidal neurons in the human superior temporal gyrus from childhood to adulthood

Nicole Barger[1,*,a], **Matthew F. Sheley**[2,b], and **Cynthia M. Schumann**[1,b]

[1]Department of Psychiatry and Behavioral Sciences, MIND Institute, University of California Davis, Sacramento, CA, 95817, USA

[2]Department of Pathology, Microbiology, and Immunology, School of Veterinary Medicine, University of California, Davis, Davis, CA, 95616, USA

Abstract

The association cortex of the superior temporal gyrus (STG) is implicated in complex social and linguistic functions. As such, reliable methods for quantifying cellular variation in this region could greatly benefit researchers interested in addressing the cellular correlates of typical and atypical function associated with these critical cognitive abilities. To facilitate this task, we first present a general set of cytoarchitectonic criteria targeted specifically toward stereological analyses of thick, Nissl stained sections for the homotypical cortex of the STG, referred to, here, as BA22/TA. Secondly, we use the optical fractionator to estimate pyramidal neuron number and the nucleator for pyramidal somal and nuclear volume to investigate the influence of age and sex on these parameters and to set a typically developing baseline for future comparisons.

In 11 typically developing cases aged 4-48 years, the most distinguishing features of BA22/TA were the presence of distinct granular layers, a prominent, jagged layer IIIc, and a distinctly staining VIa. The average number of neurons was 91 ± 15 million, volume of pyramidal soma, 1,512 μm^3, and nuclear volume, 348 μm^3. We found no correlation with age and neuron number. In contrast, pyramidal somal and nuclear volume were both negatively correlated and linearly associated with age in regression analyses. We found no significant sex differences. Overall, the data support the idea that postnatal neuron numbers are relatively stable through development but also suggest that neuronal volume may be subject to important developmental variation. Both measures are critical variables in the study of developmental neuropathology.

[*]Correspondence: Nicole Barger, Department of Psychiatry and Behavioral Sciences, UC Davis MIND Institute, 2805 50th St., Sacramento, CA, 95817, USA, nbarger@ucdavis.edu.

[a]Grant support provided by the National Institutes of Health T32 MH073124

[b]Grant support provided by National Institutes of Health R01 MH 097236 and the UC Davis MIND Institute

Conflict of Interests: The authors declare no conflict of interest with any party.

Role of Authors: All authors had full access to the data in the study and take responsibility for the integrity of the data and the accuracy of the data analysis. Study concept and design: NB and CMS. Acquisition of data: NB and MFS. Analysis and interpretation of data: NB and MFS. Drafting of the manuscript: NB and MFS. Critical revisions of the manuscript for important intellectual content: NB, MFS, and CMS. Statistical Analysis: NB Obtained funding: CMS and NB. Administrative, technical, and material support: CMS Study supervision: NB and CMS.

Keywords

temporal lobe; development; cerebral cortex; nucleator; fractionator; pyramidal neuron

I. Introduction

The homotypical association cortex covering the crown and lower wall of the superior temporal gyrus (STG), and, accordingly, the upper wall of the superior temporal sulcus (STS), is a polysensory region known to processes and integrate complex auditory, somatosensory, and visual information in human and non-human primates (Ghazanfar et al., 2005; Schönwiesner et al., 2007; Beauchamp et al., 2008; Redcay, 2008). Specific functions that consistently elicit activation in this region include speech processing, motion processing, theory of mind, audiovisual integration, gaze processing, and face processing (Allison et al., 2000; Hein and Knight, 2008; Otsuka et al., 2009). Although all of its associated functions do not necessarily fall into this domain, it appears particularly responsive to socially relevant stimuli (Allison et al., 2000; Norris et al., 2004; Lahnakoski et al., 2012). As such, it has become recognized as a critical component in the cortical circuit subserving social cognition and perception (Kennedy and Adolphs, 2012).

Historically, attempts at parcellating the cortex of the superior temporal association region have arisen from research programs with diverse objectives, making the nomenclature and parcellation schemes for this region particularly complex (Table 1). Classical anatomists interested in providing holistic parcellations of the complete cerebral cortex have consistently recognized a distinct, reasonably homogenous, strip of homotypical (six layered, granular) cortex located on the STG ventral to the lateral sulcus (Figure 1). Using cytoarchitectonic criteria, this region was designated as area 22 by Brodmann (1909) and later Sarkisov (1949), as area TA by von Economo (1929) (including caudal TA1 and rostral TA2), and type II temporal cortex by Campbell (1905) (Figure 1). Smith (1907) was able to identify a similar region in fresh brain tissue, which he described as the area temporalis superior. More recent studies have suggested further segregating the gyral and sulcal portions of these classically defined regions based on immunohistochemical (Ding et al., 2009) and autoradiographic receptor-architectonic (Morosan et al., 2005) techniques (Table 1).

An additional set of nomenclature has been introduced by analyses primarily concerned with functionally defined territories associated with auditory processing, which have been localized, experimentally, to Heschl's gyrus and adjacent regions on the dorsal wall and crown of the STG in humans (Galaburda and Sanides, 1980) (Table 1). In Galaburda and Sanides's (1980) early attempts to resolve human cytoarchitecture with the more extensive non-human primate auditory cortex literature, they described two auditory belt regions, parakoniocortical area PaAe and temporoparietal area Tpt, as corresponding to von Economo's anterior TA2 and rostral TA1, respectively (Figure 1). These parcellations have been further corroborated using immunohistochemical stains (Sweet et al., 2005). Perhaps the most extensive parcellation scheme in this vein was recently proposed by Fullerton and Pandya (2007), who designated three additional, more rostral subdivisions of homotypical cortex on the STG, including Ts1e, Ts2, and Ts3 (Table 1).

Given the functional importance of the superior temporal cortex and its relevance to multiple psychiatric and neurodevelopmental disorders (Redcay, 2008; Palaniyappan et al., 2012; Achiron et al., 2013), we sought to develop a consistent set of cytoarchitectonic criteria, based on multiple non-pathological human cases, that can easily be applied in quantitative neuroanatomical and stereological analyses. In this analysis, we targeted the homotypical association cortex located on the gyral crown of the STG and upper sulcal wall of the STS, approximating the position of von Economo's (1929) TA and Brodmann's (1909) area 22. As Brodmann's nomenclature is most commonly used and von Economo provided the most detailed criteria for delineating the region, we incorporate both authors' terminology when defining our region of interest, which we refer to as BA22/TA.

Our goal was twofold. First, we established a general set of cytoarchitectonic criteria for BA22/TA that could be applied to thick, cell-body (Nissl) stained sections based on an assessment of multiple cases at different developmental stages. Such criteria could be applied across laboratories to provide greater consistency and reproducibility of stereological results. Second, we carried out the first stereological assessment of pyramidal neuron number, somal volume, and nuclear volume in this region to provide a baseline for developmental, comparative, and neuropathological studies interested in the association cortex of the STG. Pyramidal neurons were specifically chosen as they are a common focus in the developmental and neuropathological literature, *e.g*., pyramidal neuron numbers and somal volume are altered in cases with autism spectrum disorder (van Kooten et al., 2008; Jacot-Descombes et al., 2012). We predicted that neuron numbers would fall within a similar range in children and adults, given cortical neurogenesis is considered largely completed at birth (Bhardwaj et al., 2006; Gould, 2007; Bystron et al., 2008). There is some suggestion in the literature that neuronal volume may be subject to age-related effects. However, to our knowledge, stereological analyses have not directly quantified developmental trajectories focusing only on the typically developing cerebral cortex, likely due to the limited availability of pediatric cases. Therefore, we further investigated potential variation in pyramidal somal and nuclear volume in our developmental sample.

II. Materials and Methods

Sample

This study included a complete postmortem histological series from eleven human brains 4 to 48 years of age at death with no known psychological or neurological disorder (Table 2). In no case was brain trauma the primary cause of death. Postmortem tissue was obtained from the Autism Celloidin Library (Autism Tissue Program, Autism Speaks). Donor next of kin provided all necessary written consent; the study was exempt from Internal Review Board approval.

Tissue Processing

Tissue was processed at one of two sites, the New York State Institute for Basic Research in Developmental Disabilities, Staten Island, NY, USA or the Morphologic Brain Research Unit, University of Wüerzburg, Wüerzburg, Germany. Briefly, one hemisphere from each brain was immersion-fixed in 10% formalin for at least three months prior to processing.

Subsequently, the hemispheres were celloidin embedded and sectioned at either 200, 500, or 600 μms (Table 2) to produce a 1:3 or 1:2 series. The sectioning protocol has been published previously in more detail (Heinsen and Heinsen, 1991; Heinsen et al., 2000; Wegiel et al., 2010).

Stereological Design

Prior to sampling, boundaries for BA22/TA were first determined on serial coronal sections using a Leica Wild MZ8 Stereozoom microscope, focusing between 0.63× and 5× objective. Stereological sampling was performed using a Zeiss Axio Imager.Z2 Vario microscope with an integrated camera connected to a Dell Precision T3500 Workstation, automated stage attached to a Ludl Mac6000 Stage Controller, and incorporating a Heidenhan length gage for accurate measurements in the z-axis. Boundaries were hand traced by MFS at 2.5× (N.A., 0.075) in the StereoInvestigator software program (MBF Bioscience, Williston, VT) on a regularly spaced series of 10 to 14 histological sections at distances ranging from 2,000 to 6,000 μm between sections. Detailed descriptions of our cytoarchitectonic criteria are presented in the results section.

The optical fractionator and nucleator modules of StereoInvestigator were used to estimate neuron numbers and pyramidal cell volumes, respectively (Gundersen et al., 1988; West et al., 1991). NB performed stereological sampling using a 100× (N.A., 1.4) Apochromat oil lens. Consistent with the fractionator principle, sampled sections were evenly spaced throughout the length of the entire structure with a randomly determined starting position. Post-processing section thicknesses were greater than 100 μms in all cases, providing sufficient depth for sampling (Table 3). The disector probe was set at 30 μms with 10 μm top and bottom guard zones to avoid artifacts that may result from sectioning (Dorph-Petersen et al., 2001). Prior to sampling, section thickness was systematically measured within the boundaries of BA22/TA at five sites on each section in the sample for each case using the 40× (NA, 0.74) objective. The average section thickness for each case was then used to compute stereological estimates. To achieve a systematic random sample of neurons, we ran the nucleator probe simultaneously with optical fractionator, sampling every fifth neuron. Four rays were placed emanating from the nucleolus. The intersection of the rays with the boundary of the cell nucleus and boundary of the cell soma were marked for each sampled cell. Stereological parameters are summarized in Table 3.

A cell was defined as a neuron if it contained a large, clear, lightly staining nucleus with a single distinct nucleolus, surrounded by distinct staining of the perikarya, differentiating it from other common cell types in the brain like glia or endothelial cells (Schumann and Amaral, 2005; Barger et al., 2012; Morgan et al., 2014). Pyramidal neurons were further distinguished by their large size, triangular shape, large, dark nucleolus, and the appearance of a clear apical dendrite oriented towards the pial surface and situated across from two or more basilar dendrites (Figure 2). A neuron was counted in the sample if the nucleus came into focus within the counting frame or intersecting the green lines of inclusion, but not touching the red lines of exclusion.

For cell counts and volume measurements, we differentiated pyramidal neurons in layers III, V, and VI from neurons in granular cell layers II and IV. Because the borders between

layers are not always discrete and may be distorted by gyral convolutions which are variable across cases, it can be difficult to reliably trace exact borders for each cortical layer (Jacot-Descombes et al., 2012). To address this issue, we avoided making *a priori* assumptions about the limits of these more ambiguous layer boundaries. First, we traced our boundaries for BA22/TA across the entire cortical ribbon, without subdividing the cortical layers, and densely sampled the entire region at 100×, identifying sampled pyramidal and non-pyramidal neurons with different markers. To produce estimates only for pyramidal neurons, we returned to a lower magnification (2.5 - 5×) and differentiated the cells of the granular layers, *post hoc*, similar to Schenker and Annese (2013). Previously marked pyramidal neurons falling in granular layers II and IV were re-marked as granule cells and removed from the analysis of pyramidal neurons. NB and MFS independently evaluated each case, with greater than 98% correspondence in their assessment of the layer location of all probe sites. With this sampling scheme, the average number of total neurons sampled was 544, including an average of 324 pyramidal neurons (Table 3). The coefficient of error was approximately 7% or less across all cases for the nucleator and the optical fractionator (Gundersen, m=1) (Table 3).

Reliability

MFS first performed intrarater reliability by defining the extent of BA22/TA in two independent trials for each of two cases. Volumes for the region were obtained with the Cavalieri estimator and compared across iterations. There was only a 1% difference in the total volume of the tracings across the two trials. NB then performed interrater reliability by independently tracing the region, using these cytoarchitectonic criteria, in two of the eleven cases. For both cases, there was less than a 5% difference in the total volume of regions defined by MFS and NB. Volumes were calculated only to assess the reliability of boundary definitions within individual cases since inter-subject volumetric comparisons were outside the scope of this analysis due to the potential for differential tissue shrinkage between cases (Kretschmann et al., 1982). NB performed intrarater reliability for cell counts, counting one case over 3 iterations, with less than 5% difference across trials.

Statistical Analysis

SPSS Statistics 22 (IBM, Inc.) was used to perform all analyses. All datasets passed the Kolmogrov-Smirnov test for normality. However, observation of Q-Q normality plots and histograms suggested that only somal volumes appeared normally distributed. Therefore, we chose to use non-parametric test for means comparisons and correlations. The Mann-Whitney U tests was used to compare mean values of sex and age-based subgroups. For the age comparison, we divided the sample into a pre-pubescent group, containing cases under 10 years of age, and a post-pubescent group, containing cases 14 years and over, based on the known cognitive and neuromaturational differences between these two stages (Huttenlocher and Dabholkar, 1997; Giedd et al., 1999; Gogtay et al., 2004; Shaw et al., 2008; Tau and Peterson, 2010; Petanjek et al., 2011). Spearman's rank correlation was additionally used to assess whether any of the neuronal parameters shared a significant relationship with numeric age represented as a continuous variable. Relationships found to be significant in the correlations were investigated in more detail using parametric linear regression analysis.

Photography

Nissl-stained brightfield photomicrograph images of cortical cytoarchitecture were acquired with a Nikon Photomacrography Multiphot system. Whole hemisphere images were taken with the stereological setup using the Virtual Slice module of StereoInvestigator at the 5× objective and the high magnification neuron image was taken on the same system with the 100× objective. Adobe Photoshop 10 (Adobe Systems, San Jose, CA) and GIMP 2.6.2 (http://www.gimp.org/) were used to make adjustments to brightness and contrast.

3D hemisphere reconstructions used for illustration were created as follows. For case M10-03, the post-mortem MRI was aligned in the axis that corresponded closest to the cut orientation of the coronal histological sections and a surface reconstruction was created using ITK-SNAP (www.itksnap.org) (Yushkevich et al., 2006). Boundaries for the region were approximated by transferring boundary markers from the histological section onto the corresponding MR image in the coronal plane. For the automatic sulcal parcellation, a single human subject's MRI was processed through the FreeSurfer (Fischl, 2012) 5.1 pipeline and visualized using FreeSurfer's surface viewing program (tksurfer). The Destrieux parcellations (Destrieux et al., 2010) were loaded into tksurfer to be viewed on the subject's cortical surface model and the resulting image was saved in TIFF format. To illustrate variability in the posterior extent of BA22/TA, the same MRI was processed through the FreeSurfer 5.1 pipeline. Subsequently, surfaces were exported into CARET format using the FreeSurfer to fs_LR pipeline. The resulting pial surfaces were viewed using CARET v5.64 and saved as an image. The highest dorsal extent of BA22/TA was measured on the histological sections in each case and expressed as a percent of the total hemisphere height, then computed in the space of the example brain. A transparent layer of the respective relative height was created for each case in GIMP and all cases were overlapped on the example brain to provide a basic illustration of intersubject variability.

III. Results

Cytoarchitecture

General Features—All six cortical layers are readily distinguishable in BA22/TA and exhibit a high degree of columnarity, as expected of homotypical temporal cortex. Within BA22/TA, each layer displays characteristic features (Table 1). Layer I contains loosely packed, radially oriented cells with less distinct columnarity than lower layers. In granular layer II, small cell clusters often protrude into layer I, giving this border a “frayed” appearance (*sensu* von Economo, 1929). Layer III is generally the broadest layer and appears markedly heterogeneous, exhibiting an increase in cell density and staining intensity from more cell sparse superficial portions to a dense and dark deep layer. Especially useful for distinguishing BA22/TA, this deep layer (sublayer IIIc) contains predominantly medium to large, dark staining pyramidal cells. Arranged in columns, these cells extend intermittently into IIIb, making the IIIb-IIIc boundary appear jagged and crown-like at lower magnifications. Layer IV is distinct but relatively diffuse, as its columns often bleed into the very lower margin of layer III and upper margin of V, slightly blurring these boundaries. Layer V contains especially coarse cell columns relative to the supragranular layers. Layer VI appears less columnar than V and transitions subtly into white matter. It is particularly

distinguished by the distinct, dark staining band that forms its upper sublayer (VIa), which is best visualized at low magnifications. Some variations on this standard pattern were observed rostrocaudally (Figure 3D and E). Granular layers II and IV exhibit a progressive rostral to caudal increase in staining intensity, as did layer VI. In sections roughly rostral to the start of the lateral fissure (Figure 3D), the larger cells of layer IIIc do not stain as intensely and layer V appears slightly thicker than midrostrocaudal (Figure 4A) and caudal (Figure 3E) sections.

Comparison with surrounding regions—Grossly, the columns of BA22/TA are coarser than in surrounding regions. Because they are less distinct in infra- than in supragranular layers, individual columns rarely appear to span all cortical layers, uninterrupted. BA22/TA tends to be thinner than surrounding temporal cortices, although layer III is comparatively thicker in BA22/TA. In the parietal cortex the supragranular layers are even more expanded and the infragranular layers reduced. Consequently, layer IV appears to sit relatively lower in the cortical ribbon in parietal cortex than in BA22/TA. A caveat, the relative thickness of layers can also vary as a result of systematic coronal sectioning. Across gyral convolutions, some layers can appear artificially thicker or thinner depending on the angle at which the blade ultimately crosses the cortical ribbon. Thus, regional delineations are best confirmed using multiple cytoarchitectural features of specific territories. Detailed comparisons of regional borders are listed in Table 4 and elaborated below. Particularly, differences in layers III and IV proved useful in discriminating BA22/TA from adjacent territories.

Rostral border—Area BA38/TG forms the anterior border of BA22/TA, as well as the ventromedial and dorsomedial border in the most rostral sections (Figure 3C; Figure 5A). Dysgranular BA38/TG exhibits a poorly developed, incipient layer IV and a thin (approximately 4-6 pyramidal cells thick) layer II, unlike granular BA22/TA. Additionally, layer II appears as a darkly staining band, occasionally interrupted by cell sparse regions, that appears to “cap” the lower cortical layers. In layer III, BA38/TG shows more of a graded transition in cell size and density from superficial to deep layers, contrasting with the more stratified III of BA22/TA. In some cases, layer VIa was observed to stain more intensely than in BA22/TA.

Caudal border—The parietal cortex of area BA40/PF forms the caudal border of BA22/TA (Figure 3F; Figure 5F). Cortical columns are finer and more discrete in BA40/PF and run uninterrupted from layers II-VI. Layer II appears thicker and the transition into layer III is more gradual than in BA22/TA. Layer IIIc is also distinct and dark but appears more as a band or stripe, as pyramidal neurons are predominantly confined to layer IIIc.

Ventromedial border—In every case, the homotypical cortical area BA21/TE forms the entire ventromedial border of BA22/TA caudal to BA38/TG (Figure 4C; Figure 5B-F). In BA21/TE, the large, dark staining cells of layer III are present in IIIc but also can be found in lower densities in all sublayers, which is unusual in BA22/TA. In BA21/TE, layer IV appears more discrete, forming a thin, compact band of tissue. Sublayers of VI are less clearly differentiated in area BA21/TE.

Dorsomedial border—The more granulous regions BA41/TB (Figure 4B) and, much less frequently BA41/TC, form the dorsomedial border of BA22/TA intermediate to rostral area BA38/TG and caudal area BA40/PF (Figure 5B-E). Overall, these regions appear more markedly columnar than BA22/TA and individual columns could be traced across all cortical layers, the classic “organ-pipe” appearance first noted by von Economo (1929). The granular layers II and IV are noticeably broad and clearly intermix with adjacent cortical layers. In layer III, the large pyramidal cells are more dispersed and sublayers less easily visualized. Layer V is less cell dense than in BA22/TA, appearing as a light band. Layer VI can appear darker in BA41/TB than in BA22/TA, but this was not visible in every case.

Gross location

After assessing boundaries for this region across the eleven cases, we found that the six layered homotypical cortex of the STG is located in a position similar to Brodmann's area 22 and von Economo's area TA, extending from the dome of the STG onto its ventral wall towards the fundus of the STS. Rostrally, the cytoarchitectural region tends to form within the first 2.5 mm of the start of the STG. Rarely, BA22/TA may form slightly rostral the rostral extent of the gyrus, but this was observed in fewer than 20% of cases. At this level, BA22/TA is commonly bordered on all sides by BA38/TG and is rostral to the middle temporal gyrus, containing BA21/TE. More caudally, BA21/TE forms the ventromedial border, near the fundus of the STS, tending in most cases to encroach slightly onto the ventral wall of the STS. Prior to the formation of the limen insula, the dorsomedial limit tends to extend around the crown of the STG. More caudally, as the insular and auditory cortices of the superior temporal plane develop, BA22/TA appears more laterally, approximately where the crown of the STG meets the ventral wall of the lateral fissure (Figure 5B-E). In the caudal-most sections, BA22/TA extends past the closure of the lateral fissure and, at that point, commonly continues caudally and transitions into the inferior parietal lobule, usually ending just prior to the closure of the STS.

Neuron numbers

The average number of pyramidal neurons across cases was 90.98 ± 14.88 million in BA22/TA. Pyramidal neuron numbers for each case are summarized in Table 5. Neuron number did not show any relationship with age (r_s = 0, p = 1.00) (Figure 6) nor did mean neuron number vary between sexes (U = 19, p = 0.54).

Neuron volumes

Across cases, the average volume of neuronal soma and nuclei were 1,512 μm^3 and 348 μm^3, respectively. Individual volumes for neuronal soma and neuronal nuclei are presented in Table 5. Significant negative correlations with age were found for whole pyramidal somal volume ($r_{s=}$ -0.62, p = 0.04) and nuclear volume ($r_{s=}$ -0.70, p = 0.02). In regression analyses (Figure 7), increased age also appeared to be a significant predictor of reduced somal volume (y = 1755.04 -14.85×, R^2 = 0.48, p = 0.02) and nuclear volume (y = 425.04 - 4.71×, R^2 = 0.37, p = 0.05). The average somal volume for pre-pubescent cases (< 10 years of age) was 1,708 μm^3 and differed significantly from the post-pubescent average which was 1,349 μm^3 (U = 3; p = 0.03). Pre-pubescent cases' average nuclear volume, 415 μm^3, was not

significantly different from post-pubescent volumes, 291 μm^3, (U = 5, p = 0.08). Somal volume was not significantly larger in females than in males in the sample (U = 5, $p = 0.08$), nor was nuclear volume (U = 10, $p = 0.43$).

IV. Discussion

Using a consistent set of cytoarchitectural definitions suitable for performing modern stereological analyses on thick sections, we found that the average number of neurons in the homotypical cortical territory BA22/TA of the human STG is approximately 91 (± 15) million in cases ranging from 4 to 48 years of age at death. The average volume of pyramidal soma is 1,512 μm^3 and nuclei is 348 μm^3. However, in this sample, the size of the pyramidal soma and nuclei exhibited a negative relationship with age. The five younger, pre-pubescent, cases had a significantly higher average somal volume, 1,708 μms^3, than post-pubescent cases, 1,349 μms^3.

Comparison with previous studies of cytoarchitecture

As stereological methods increasingly become the standard in comparative and neuropathological studies, there is a growing practical need for descriptions of cytoarchitecture in thick sections. Classical cytoarchitectural mapping derived from thin sections cannot always readily be applied to thicker, more darkly-stained tissue. This is further complicated by the fact that classical studies often focused on the optimal visualization of a portion of a region, rather than delineating the entire rostrocaudal extent of the region as required for systematic stereological sectioning and sampling. Consistent with the complex systems of nomenclature proposed for this region, a complex set of cytoarchitectural descriptions of the homotypical cortex of the STG has been presented in the literature (Table 1). In thick sections, we found a certain set of features to be reliably present across multiple human cases. They are largely consistent with prior cytoarchitectural assessments based on thinner-sectioned tissue and are visible in thinner-sectioned series in our own collection.

A summary of cytoarchitectural features of the STG described in previous studies are presented in Table 1. von Economo's (1929) observations for parcellating the STG generally provided the most consistent guide, with a few notable differences. In agreement with von Economo and others, we found this region to be distinguished as both clearly homotypical and coarsely columnar. Numerous authors report granular layers II and IV in this region are distinct, thicker than in temporal polar cortex (von Economo, 1929; Morosan et al., 2005; Fullerton and Pandya, 2007; Ding et al., 2009; Blaizot et al., 2010; Insausti, 2013), and thinner than in auditory regions (Smith, 1907; von Economo, 1929; Galaburda and Sanides, 1980; Morosan et al., 2005; Fullerton and Pandya, 2007). As observed in other analyses, layer IV appeared particularly columnar in organization (Campbell, 1905; von Economo, 1929; Blaizot et al., 2010) with poorly defined boundaries that tended to blend into III and V (Galaburda and Sanides, 1980; Sweet et al., 2005; Fullerton and Pandya, 2007). Across authors, there is little disagreement that layer VI is fairly cell dense (von Economo, 1929; Galaburda and Sanides, 1980; Ding et al., 2009; Blaizot et al., 2010), exhibiting a gradual transition to the cerebral white matter (von Economo, 1929; Morosan et al., 2005).

One point of difference, while von Economo noted that layer I of TA is thick, we found layer I generally unremarkable and not especially thicker than surrounding regions, in agreement with much of the literature (Campbell, 1905; Galaburda and Sanides, 1980; Morosan et al., 2005; Sweet et al., 2005; Fullerton and Pandya, 2007; Ding et al., 2009; Blaizot et al., 2010). While von Economo referred to layer III as generally uniform, we found the dark, often jagged sublayer IIIc to be particularly useful in differentiating this region from surrounding areas. Similarly, Galaburda and Sanides (1980) noted the prominence of IIIc cells in this region, describing their area PaAe (in a similar location as von Economo's rostral TA2) as containing distinct columns of medium sized pyramidals 3-8 cells deep in the deeper parts of layer III, and Tpt (in a similar location as caudal TA1) as exhibiting a distinct layer IIIc with an undulating, irregular border. Morosan and colleagues (2005) also noted the prominence of layer IIIc and its dark cell columns in their description of the cytoarchitecture of area Te3, corresponding to the gyral dome area of our BA22/TA (Table 1). In the temporal polar region, Blaizot and colleagues (2010) as well as Insausti (2013) note that layer III exhibits a more subtle cellular gradient, with cells progressively increasing in size from superficial to deep portions of the layer, and reduced columnarity compared to BA22/TA. Thus, a number of authors have additionally found the sublayers of IIIc to be useful in differentiating this region from surrounding territories.

In agreement with others, we observed slight variations in cytoarchitecture in rostral relative to caudal regions. Rostrally, we found layer VI appeared less distinct, and other authors have observed that the border between layers V and VI appears more subtle (Ding et al., 2009) and less apparent (Fullerton and Pandya, 2007) in rostral subdivisions. Cells of IIIc also tended to be less distinct, anteriorly (Figure 3). Accordingly, Fullerton and Pandya (2007) describe IIIc as dark staining in more caudal regions but not in their rostral subdivisions. von Economo (1929) noted other variation in the rostrocaudal dimension, specifically an increase in the size of layer V, rostrally, as well as an increase in cell size and morphology. We also noted a small increase in thickness of layer V, but did not observe any changes in cell size or morphology nor have other authors noted this distinction in layer V cells.

Gross topographical extent of the region

In its gross location, we found that our cytoarchitectonically defined region, BA22/TA, corresponded well with classical descriptions of the caudal extent of the region but extended slightly further, rostrally. Brodmann (1909) and Campbell (1905) both locate the rostral boundary of their regions, area 22 and type II temporal cortex respectively, where the ventral aspect of the central sulcus meets the STG. Von Economo (1929) placed his boundary slightly more anteriorly, but after the start of the STS (Figure 1). In contrast, we found the region generally began within a few millimeters of the formation of the STS or slightly further rostrally and was commonly surrounded completely by BA38/TG. This is in closer agreement with recent analyses focusing on the temporal polar region (Table 1), anterior to the limen insula, which describe a cytoarchitecturally similar region in the portion of the STG originally defined as temporal polar area TG (Ding et al., 2009; Blaizot et al., 2010). Indeed, in a later assessment of 14 separate hemispheres, von Economo and Horn (1930) do illustrate a subparcellation of area TA, TA2(G), extending into the superior temporal gyral constituents of the temporal polar region in some cases. Both Brodmann and

von Economo's textual descriptions indicate that areas 22 and TA can extend caudally and dorsally into the parietal lobule, although it may not be readily apparent on classical maps. In agreement, we found BA22/TA often transitioned into the gross territory of the supramarginal gyrus and ended just prior to the closure of the STS (Figure 8). Galaburda and Sanides (1980) similarly considered the posterior extent of area Tpt to include “variable” amounts of the suprasylvian cortex and portions of the inferior parietal lobule.

Our definitions of the ventromedial and dorsomedial extent of BA22/TA are in general agreement with classical studies, which group together the cortex of the dome of the STG and the upper wall of the STS (Campbell, 1905; Brodmann, 1909; von Economo, 1929). Rostrally, prior to the formation of the limen insula, the dorsomedial border extends medial to the crown of the STG (Figure 5A), but, as the insular and auditory cortices develop, the dorsomedial border moves laterally to the junction of the crown of the STG and the ventral lateral fissure (Figure 5B-E). Caudal to the temporal pole (BA21/TE), the fundus of the STS marks the ventromedial border, but the region may extend slightly onto the ventral wall of the STS (Figure 5C & D). Studies incorporating chemical techniques have argued for segregating the gyral crown and sulcal wall into distinct territories, citing some corresponding variation in cytoarchitecture (Morosan et al., 2005; Ding et al., 2009). While we noted subtle differences in the cytoarchitecture in the gyral and sulcal territories, we, like von Economo, did not see substantial differences present in all cases.

Understanding the exact topographic extent of cytoarchitecturally distinct regions is critical for interpreting neuroimaging data, which is more typically reliant on gross sulcal landmarks. From our observations of the extent of the cytoarchitectural region, it is possible that MRI parcellation schemes that use sulcal markers to define territories, *e.g.*, FreeSurfer, may provide a good approximation of the rostral extent of the cytoarchitectural region (Figure 8). However, because the posterior border frequently transitions into the inferior parietal lobule, gyral morphology is less likely to reflect true cytoarchitectural boundaries of posterior BA22/TA in some cases (Figure 8). It may be more often included in inferior parietal cortex or a transitional zone, such as the temporoparietal junction.

Comparison with previous stereological studies

We are unaware of any prior stereological analysis of the region we have defined, BA22/TA. The total number of neurons in the entire temporal lobe has been estimated to be approximately 4.3 billion neurons total (averaged across sexes) (Pakkenberg and Gundersen, 1997). The entorhinal cortex contains approximately 13 million neurons, with 12 million residing in layers III, V, and VI (West and Slomianka, 1998). The temporal polar cortex (BA38) has been reported to contain 103 million neurons in typical cases (Bothwell et al., 2001). We found the average number of pyramidal neurons in layers III, V, and VI of BA22/TA to be slightly less, approximately 91 million, despite the larger expanse of BA22/TA. Although the number of neurons falling in the granular cell layers did not reach a sufficient coefficient of error in all cases and were, consequently, not reported, in the 7 cases with a CE of 0.08 or less, the average number of granule cell neurons was approximately 54 million and the average number of granule and pyramidal neurons together in these 7 cases was approximately 145 million. This number is in line with other findings for the temporal

pole, especially considering non-pyramidal neurons, like cortical interneurons and fusiform cells, would also contribute to the total neuron number. Cortical pyramidal neuron somal volumes are close to those reported for other regions utilizing the same brain tissue collection as our study (van Kooten et al., 2008; Jacot-Descombes et al., 2012; Uppal et al., 2014).

Age-related variation in neuronal parameters

Because it is widely accepted that cortical neurogenesis is largely complete or occurring only at low rates in human and non-human primate postnatal development (Rakic, 2002; Uylings et al., 2005; Bhardwaj et al., 2006; Gould, 2007; Zhao et al., 2008), we expected to see little to no evidence of age-related changes in neuron number in our developmental sample. However, few analyses which have directly investigated this theory by quantifying changes in neuron number through human cortical development are available for comparison. One prior analysis has presented evidence in favor of age-related increase in human cortical neuron numbers in early postnatal development using data that was carried out prior to the use of more modern assumption-free stereological methods (Shankle et al., 1999), while another has disputed this finding in a stereological analysis of Broca's Area (Uylings et al., 2005). Our findings in the STG are in agreement with the latter stereological analysis, evidencing consistency across stereological studies. Accordingly, our data further support the idea that conservative rates of cortical neurogenesis are occurring postnatally, at least in the STG in the developmental period from early childhood to adulthood.

In contrast, we found a negative relationship between age and pyramidal neuron volume from childhood to adulthood. The availability of data on human cellular development in the transitional period between childhood and adolescence is limited (Tau and Peterson, 2010). Even fewer studies have employed unbiased stereological methods to assess developmental changes in this period. However, two recent stereological analyses focusing on autistic neuropathology report similar trends in many brain structures in their control samples (Jacot-Descombes et al., 2012; Wegiel et al., 2014). Most relevant, in another language-associated region, Brodmann's areas 44 and 45, typically developing control cases evidenced a significant negative relationship between age and pyramidal neuron volumes in layers III and VI (Jacot-Descombes et al., 2012). Additionally, several subcortical structures, including the thalamus, all components of the striatum, claustrum, and dentate gyrus, have been reported to exhibit decreased neuron volumes in older cases compared to children in the sample (Wegiel et al., 2014). It should be noted that each of these studies also used the Autism Celloidin Library (ACL), one of the few collections which has a comparatively large typically developing pediatric sample. Given that all three studies used the same collection and that sample sizes are limited by a number of factors in human postmortem analyses, it may be the case that our converging results reflect a sample bias, if the common developmental sample used is not representative of the true population distribution. While possible, we think that this is unlikely to account solely for similar results across studies, as each study used a distinct subsample of the ACL and only three individual cases were used in all three analyses (M3-04, F 8 y.o., 444-02, M 23 y.o., and M10-03, M 48 y.o.). Added support comes from an independent analysis of Golgi stained tissue, which reported a transient increase in pyramidal somal surface area in early childhood in the prefrontal

association cortex, around six years of age, which was substantially greater than in late childhood and early adolescence (Petanjek et al., 2008).

Given analyses using different samples converge on a common finding, it is tempting to regard the observed trend towards somal decrease from early childhood to adulthood as a novel and potentially critical contribution to this poorly understood period of cellular development. We speculate that larger volumes in middle and late childhood reflect the somal response to a heightened period of synaptic proliferation in early development, while subsequent somal decrease correlates with synaptic refinement as cortical circuits mature. In terms of overall brain growth, the period of late childhood is generally regarded as a 'plateau' period with reduced rates of volumetric expansion compared to infancy (Tau and Peterson, 2010). Yet, some late maturing portions of the cortex, including the STG, continue to expand well into this period (Gogtay et al., 2004). Moreover, in childhood, substantial modifications to dendritic and synaptic morphology (Huttenlocher and Dabholkar, 1997; Petanjek et al., 2011) occur in tandem with increased rates of aerobic glycolysis (Goyal et al., 2014) theorized to provide anabolic support for this active period of cellular development (Bauernfeind et al., 2014). As neuronal and nuclear volume are traditionally thought to reflect metabolic activity in the cell (Schmitz et al., 1999), heightened neurodevelopmental activity may be associated with a concomitant increase in cell volume. Accordingly, in the prefrontal association cortex, childhood increase in somal volume (Petanjek et al., 2008) roughly parallels an exuberant period of dendritic spine proliferation (Petanjek et al., 2011). By late childhood and early adolescence, gross cortical volume begins to decline, especially in portions of the posterior STG (Mills et al., 2014). The cellular underpinnings of this trend remain largely unexamined (Gogtay et al., 2004; Tau and Peterson, 2010), but our data support the proposition that cell shrinkage may contribute to this process (Gogtay et al., 2004).

Similar to gross volumetric trends observed in neuroimaging (Mills et al., 2014), we found cases under 10 years of age exhibit significantly greater somal volumes than older cases likely due to a pattern of gradual developmental decrease from childhood to adulthood (Figure 7), which may also reflect events at the synaptic level as dendritic spines are pruned in later development (Gogtay et al., 2004). Increased sample sizes are needed to further substantiate the interesting finding that neuronal volume in childhood is particularly increased relative to adult volume and to optimally characterize the developmental trajectory of pyramidal neuron somal volume.

Broader significance

The STG is involved in important higher order social cognitive and linguistic functions that are particularly essential to complex human social cognition (Herrmann et al., 2007; Dunbar, 2009). It is activated in socially meaningful aspects of speech, like speaker recognition (Kriegstein and Giraud, 2004), while synchronous activation of this region between listeners and speakers is associated with variables related to communicative success (Dikker et al., 2014). Theory of mind tasks generally evoke activation in this region across subjects (Hein and Knight, 2008), and inter-individual differences in performance on theory of mind tasks may be explained by activation levels in the STG more than other neural territories (Otsuka

et al., 2009). Structurally, cortical density in the STG has been shown to correlate with social network sizes (Kanai and Bahrami, 2012). In comparative neuroimaging experiments, the temporal lobe and STG evidence significant expansion in humans relative to other primates (Rilling and Seligman, 2002; Hill et al., 2010), while homologous cytoarchitectonic regions have been reported in non-human primates (Hackett et al., 2001; Fullerton and Pandya, 2007; Spocter et al., 2010). As such, stereological studies using similar parameters as ours to investigate the neural underpinnings of human volumetric deviations from our closest relatives, the apes, could greatly contribute to our understanding of the evolution of the human brain and complex social cognition.

The lateral temporal cortex exhibits one of the most protracted growth periods in the brain (Giedd et al., 1999; Gogtay et al., 2004; Mills et al., 2014), and volumetric developmental increases in this region are on par with increases in the dorsolateral prefrontal cortex from infancy to adulthood (Hill et al., 2010). From a neuropathological perspective, a long and complex period of substantial growth may make late maturing structures more susceptible to postnatal developmental insult at multiple developmental stages and more affected by early disruptions in typical development (Hill et al., 2010). Indeed, several debilitating cognitive disorders are linked to STG dysfunction (Garbett et al., 2008; Redcay, 2008; Palaniyappan et al., 2012; Achiron et al., 2013). Consistent with the STG's role in social behavior, increasing evidence implicates functional and neural pathology of the STG in autism spectrum disorder (Zilbovicius et al., 2006; Redcay, 2008). At the molecular level, this region also displays differential expression of gene transcripts related to immune function (Garbett et al., 2008) and of small non-coding RNAs (Ander et al., 2013; Stamova et al., 2014) in autistic compared with typically developing cases. Additionally, reduced STG volume has been associated with the severity of auditory hallucinations in schizophrenia (Palaniyappan et al., 2012), and it was the only region of the brain exhibiting a negative correlation between cortical thickness and cognitive performance in multiple sclerosis (Achiron et al., 2013). Stereological investigations of the region defined as BA22/TA can provide important information about the effect of variation at the cellular level on these and other gross pathologies.

Acknowledgments

This work was supported by the National Institute of Health and the UC Davis MIND Institute. We thank Dr. Jane Pickett and the Autism Brain Net (formerly ATP, Autism Speaks) for providing access to cases as well as the donors and their families for their generous donations. We would like to additionally thank Aaron Lee for assistance with image preparation and Martha Vargas for laboratory support.

Literature Cited

Achiron A, Chapman J, Tal S, Bercovich E, Gil H, Achiron A. Superior temporal gyrus thickness correlates with cognitive performance in multiple sclerosis. Brain Struct Funct. 2013; 218:943–50. [PubMed: 22790785]

Allison T, Puce A, McCarthy G. Social perception from visual cues: role of the STS region. Trends Cogn Sci. 2000; 4:267–78. [PubMed: 10859571]

Ander BP, Barger N, Stamova B, Sharp FR, Schumann CM. Region-specific differences in small non-coding RNA expression in the cortex of autism brain. Neurosci Meet Planner San Diego, CA Soc Neurosci 2013. 2013 Program No. 692.05. Online.

Barger N, Stefanacci L, Schumann CM, Sherwood CC, Annese J, Allman JM, Buckwalter JA, Hof PR, Semendeferi K. Neuronal populations in the basolateral nuclei of the amygdala are differentially increased in humans compared with apes: a stereological study. J Comp Neurol. 2012; 520:3035–54. [PubMed: 22473387]

Bauernfeind AL, Barks SK, Duka T, Grossman LI, Hof PR, Sherwood CC. Aerobic glycolysis in the primate brain: reconsidering the implications for growth and maintenance. Brain Struct Funct. 2014; 219:1149–67. [PubMed: 24185460]

Beauchamp MS, Yasar NE, Frye RE, Ro T. Touch, sound and vision in human superior temporal sulcus. Neuroimage. 2008; 41:1011–1020. [PubMed: 18440831]

Bhardwaj RD, Curtis MA, Spalding KL, Buchholz BA, Fink D, Björk-Eriksson T, Nordborg C, Gage FH, Druid H, Eriksson PS, Frisén J. Neocortical neurogenesis in humans is restricted to development. Proc Natl Acad Sci U S A. 2006; 103:12564–8. [PubMed: 16901981]

Blaizot X, Mansilla F, Insausti AM, Constans JM, Salinas-Alamán A, Pró-Sistiaga P, Mohedano-Moriano A, Insausti R. The human parahippocampal region: I. Temporal pole cytoarchitectonic and MRI correlation. Cereb Cortex. 2010; 20:2198–212. [PubMed: 20064939]

Bothwell S, Meredith GE, Phillips J, Stanton H, Doherty C, Grigorenko E, Glazier S, Deadwyler SA, O'Donovoan CA, Farrell M. Neuronal hypertrophy in the neocortex of patients with temporal lobe epilepsy. J Neurosci. 2001; 21:4789–800. [PubMed: 11425906]

Brodmann, K. Localisation in the Cerebral Cortex. Gordon, Smith, editor. London, UK: 1909.

Bystron I, Blakemore C, Rakic P. Development of the human cerebral cortex: Boulder Committee revisited. Nat Rev Neurosci. 2008; 9:110–22. [PubMed: 18209730]

Campbell, AW. Histological studies on the localisation of cerebral function. Cambridge: Cambridge Univ Press; 1905.

Destrieux C, Fischl B, Dale A, Halgren E. Automatic parcellation of human cortical gyri and sulci using standard anatomical nomenclature. Neuroimage. 2010; 53:1–15. [PubMed: 20547229]

Dikker S, Silbert LJ, Hasson U, Zevin JD. On the same wavelength: predictable language enhances speaker-listener brain-to-brain synchrony in posterior superior temporal gyrus. J Neurosci. 2014; 34:6267–72. [PubMed: 24790197]

Ding SL, Van Hoesen GW, Cassell MD, Poremba A. Parcellation of human temporal polar cortex: a combined analysis of multiple cytoarchitectonic, chemoarchitectonic, and pathological markers. J Comp Neurol. 2009; 514:595–623. [PubMed: 19363802]

Dorph-Petersen KA, Nyengaard JR, Gundersen HJG. Tissue shrinkage and unbiased stereological estimation of particle number and size*. J Microsc. 2001; 204:232–246. [PubMed: 11903800]

Dunbar RIM. The social brain hypothesis and its implications for social evolution. Ann Hum Biol. 2009; 36:562–72. [PubMed: 19575315]

von Economo C, Horn L. Über Windungsrelief, Maße und Rindenarchitektonik der Supratemporalfläche, ihre individuellen und ihre Seitenunterschiede. Zeitschrift für die gesamte Neurol und Psychiatr. 1930; 130:678–757.

von Economo, C. Cytoarchitonics of the human cerebral cortex. London, UK: Oxford University Press; 1929.

Fischl B. FreeSurfer. Neuroimage. 2012; 62:774–81. [PubMed: 22248573]

Fullerton BC, Pandya DN. Architectonic analysis of the auditory-related areas of the superior temporal region in human brain. J Comp Neurol. 2007; 504:470–498. [PubMed: 17701981]

Galaburda A, Sanides F. Cytoarchitectonic organization of the human auditory cortex. J Comp Neurol. 1980; 190:597–610. [PubMed: 6771305]

Garbett K, Ebert PJ, Mitchell A, Lintas C, Manzi B, Mirnics K, Persico AM. Immune transcriptome alterations in the temporal cortex of subjects with autism. Neurobiol Dis. 2008; 30:303–11. [PubMed: 18378158]

Ghazanfar AA, Maier JX, Hoffman KL, Logothetis NK. Multisensory integration of dynamic faces and voices in rhesus monkey auditory cortex. J Neurosci. 2005; 25:5004–5012. [PubMed: 15901781]

Giedd JN, Blumenthal J, Jeffries NO, Castellanos FX, Liu H, Zijdenbos A, Paus T, Evans AC, Rapoport JL. Brain development during childhood and adolescence: a longitudinal MRI study. Nat Neurosci. 1999; 2:861–3. [PubMed: 10491603]

Gogtay N, Giedd JN, Lusk L, Hayashi KM, Greenstein D, Vaituzis AC, Nugent TF, Herman DH, Clasen LS, Toga AW, Rapoport JL, Thompson PM. Dynamic mapping of human cortical development during childhood through early adulthood. Proc Natl Acad Sci U S A. 2004; 101:8174–9. [PubMed: 15148381]

Gould E. How widespread is adult neurogenesis in mammals? Nat Rev Neurosci. 2007; 8:481–8. [PubMed: 17514200]

Goyal MS, Hawrylycz M, Miller JA, Snyder AZ, Raichle ME. Aerobic glycolysis in the human brain is associated with development and neotenous gene expression. Cell Metab. 2014; 19:49–57. [PubMed: 24411938]

Gundersen HJ, Bagger P, Bendtsen TF, Evans SM, Korbo L, Marcussen N, Møller A, Nielsen K, Nyengaard JR, Pakkenberg B. The new stereological tools: disector, fractionator, nucleator and point sampled intercepts and their use in pathological research and diagnosis. APMIS. 1988; 96:857–81. [PubMed: 3056461]

Hackett TA, Preuss TM, Kaas JH. Architectonic identification of the core region in auditory cortex of macaques, chimpanzees, and humans. J Comp Neurol. 2001; 441:197–222. [PubMed: 11745645]

Hein G, Knight RT. Superior temporal sulcus--It's my area: or is it? J Cogn Neurosci. 2008; 20:2125–2136. [PubMed: 18457502]

Heinsen H, Arzberger T, Schmitz C. Celloidin mounting (embedding without infiltration) - a new, simple and reliable method for producing serial sections of high thickness through complete human brains and its application to stereological and immunohistochemical investigations. J Chem Neuroanat. 2000; 20:49–59. [PubMed: 11074343]

Heinsen H, Heinsen YL. Serial thick, frozen, gallocyanin stained sections of human central nervous system. J Histotechnol. 1991; 14:167–173.

Herrmann E, Call J, Hernàndez-Lloreda MV, Hare B, Tomasello M. Humans have evolved specialized skills of social cognition: the cultural intelligence hypothesis. Science. 2007; 317:1360–6. [PubMed: 17823346]

Hill J, Inder T, Neil J, Dierker D, Harwell J, Van Essen D. Similar patterns of cortical expansion during human development and evolution. Proc Natl Acad Sci U S A. 2010; 107:13135–40. [PubMed: 20624964]

Huttenlocher PR, Dabholkar AS. Regional differences in synaptogenesis in human cerebral cortex. J Comp Neurol. 1997; 387:167–78. [PubMed: 9336221]

Insausti R. Comparative neuroanatomical parcellation of the human and nonhuman primate temporal pole. J Comp Neurol. 2013; 521:4163–76. [PubMed: 23881792]

Jacot-Descombes S, Uppal N, Wicinski B, Santos M, Schmeidler J, Giannakopoulos P, Heinsen H, Heinsein H, Schmitz C, Hof PR. Decreased pyramidal neuron size in Brodmann areas 44 and 45 in patients with autism. Acta Neuropathol. 2012; 124:67–79. [PubMed: 22467063]

Kanai R, Bahrami B. Online social network size is reflected in human brain structure. Proc R Soc Ser B Biol Sci. 2012; 279:1327–1334.

Kennedy DP, Adolphs R. The social brain in psychiatric and neurological disorders. Trends Cogn Sci. 2012; 16:559–72. [PubMed: 23047070]

van Kooten IAJ, Palmen SJMC, von Cappeln P, Steinbusch HWM, Korr H, Heinsen H, Hof PR, van Engeland H, Schmitz C. Neurons in the fusiform gyrus are fewer and smaller in autism. Brain. 2008; 131:987–99. [PubMed: 18332073]

Kretschmann HJ, Tafesse U, Herrmann A. Different volume changes of cerebral cortex and white matter during histological preparation. Microsc Acta. 1982; 86:13–24. [PubMed: 7048029]

Kriegstein KV, Giraud AL. Distinct functional substrates along the right superior temporal sulcus for the processing of voices. Neuroimage. 2004; 22:948–955. [PubMed: 15193626]

Lahnakoski JM, Glerean E, Salmi J, Jääskeläinen IP, Sams M, Hari R, Nummenmaa L. Naturalistic fMRI mapping reveals superior temporal sulcus as the hub for the distributed brain network for social perception. Front Hum Neurosci Neurosci. 2012; 6:1–14.

Mills KL, Lalonde F, Clasen LS, Giedd JN, Blakemore SJ. Developmental changes in the structure of the social brain in late childhood and adolescence. Soc Cogn Affect Neurosci. 2014; 9:123–31. [PubMed: 23051898]

Morgan JT, Barger N, Amaral DG, Schumann CM. Stereological Study of Amygdala Glial Populations in Adolescents and Adults with Autism Spectrum Disorder. PLoS One. 2014; 9:e110356. [PubMed: 25330013]

Morosan P, Schleicher A, Amunts K, Zilles K. Multimodal architectonic mapping of human superior temporal gyrus. Anat Embryol (Berl). 2005; 210:401–6. [PubMed: 16170539]

Norris CJ, Chen EE, Zhu DC, Small SL, Cacioppo JT. The interaction of social and emotional processes in the brain. J Cogn Neurosci. 2004; 16:1818–29. [PubMed: 15701231]

Otsuka Y, Osaka N, Ikeda T, Osaka M. Individual differences in the theory of mind and superior temporal sulcus. Neurosci Lett. 2009; 463:150–153. [PubMed: 19632299]

Pakkenberg B, Gundersen H. Neocortical neuron number in humans: effect of sex and age. J Comp Neurol. 1997; 384:312–320. [PubMed: 9215725]

Palaniyappan L, Balain V, Radua J, Liddle PF. Structural correlates of auditory hallucinations in schizophrenia: a meta-analysis. Schizophr Res. 2012; 137:169–73. [PubMed: 22341902]

Petanjek Z, Judas M, Kostović I, Uylings HBM. Lifespan alterations of basal dendritic trees of pyramidal neurons in the human prefrontal cortex: a layer-specific pattern. Cereb Cortex. 2008; 18:915–29. [PubMed: 17652464]

Petanjek Z, Judaš M, Šimic G, Rasin MR, Uylings HBM, Rakic P, Kostovic I. Extraordinary neoteny of synaptic spines in the human prefrontal cortex. Proc Natl Acad Sci U S A. 2011; 108:13281–6. [PubMed: 21788513]

Rakic P. Adult neurogenesis in mammals: an identity crisis. J Neurosci. 2002; 22:614–8. [PubMed: 11826088]

Redcay E. The superior temporal sulcus performs a common function for social and speech perception: implications for the emergence of autism. Neurosci Biobehav Rev. 2008; 32:123–42. [PubMed: 17706781]

Rilling JK, Seligman RA. A quantitative morphometric comparative analysis of the primate temporal lobe. J Hum Evol. 2002; 42:505–33. [PubMed: 11969295]

Sarkisov, SA.; Filimonoff, IN.; Preobrashenskaya, IS. Cytoarchitecture of the human cortex cerebri. Moscow: Medzig; 1949.

Schenker-Ahmed NM, Annese J. Cortical mapping by magnetic resonance imaging (MRI) and quantitative cytological analysis in the human brain: a feasibility study in the fusiform gyrus. J Neurosci Methods. 2013; 218:9–16. [PubMed: 23628159]

Schmitz C, Schuster D, Niessen P, Korr H. No difference between estimated mean nuclear volumes of various types of neurons in the mouse brain obtained on either isotropic uniform random sections or conventional frontal or sagittal sections. J Neurosci Methods. 1999; 88:71–82. [PubMed: 10379581]

Schönwiesner M, Novitski N, Pakarinen S, Carlson S, Tervaniemi M, Näätänen R. Heschl's gyrus, posterior superior temporal gyrus, and mid-ventrolateral prefrontal cortex have different roles in the detection of acoustic changes. J Neurophysiol. 2007; 97:2075–82. [PubMed: 17182905]

Schumann CM, Amaral DG. Stereological estimation of the number of neurons in the human amygdaloid complex. J Comp Neurol. 2005; 491:320–9. [PubMed: 16175550]

Shankle WR, Rafii MS, Landing BH, Fallon JH. Approximate doubling of numbers of neurons in postnatal human cerebral cortex and in 35 specific cytoarchitectural areas from birth to 72 months. Pediatr Dev Pathol. 1999; 2:244–59. [PubMed: 10191348]

Shaw P, Kabani NJ, Lerch JP, Eckstrand K, Lenroot R, Gogtay N, Greenstein D, Clasen L, Evans A, Rapoport JL, Giedd JN, Wise SP. Neurodevelopmental trajectories of the human cerebral cortex. J Neurosci. 2008; 28:3586–94. [PubMed: 18385317]

Smith G. A new topographical survey of the human cerebral cortex, being an account of the distribution of the anatomically distinct cortical areas and their relationship to the cerebral sulci. J Anat Physiol. 1907; 61:237–254. [PubMed: 17232738]

Spocter MA, Hopkins WD, Garrison AR, Bauernfeind AL, Stimpson CD, Hof PR, Sherwood CC. Wernicke's area homologue in chimpanzees (Pan troglodytes) and its relation to the appearance of modern human language. Proc Biol Sci. 2010; 277:2165–74. [PubMed: 20236975]

Stamova B, Ander BP, Barger N, Sharp FR, Schumann CM. ncRNA expression differs more with age and by region in typical brain development than in ASD. Neurosci Meet Planner San Diego, CA Soc Neurosci 2014. 2014 604.12/J2. Online.

Sweet RA, Dorph-Petersen KA, Lewis DA. Mapping auditory core, lateral belt, and parabelt cortices in the human superior temporal gyrus. J Comp Neurol. 2005; 491:270–89. [PubMed: 16134138]

Tau GZ, Peterson BS. Normal development of brain circuits. Neuropsychopharmacology. 2010; 35:147–68. [PubMed: 19794405]

Uppal N, Gianatiempo I, Wicinski B, Schmeidler J, Heinsen H, Schmitz C, Buxbaum JD, Hof PR. Neuropathology of the posteroinferior occipitotemporal gyrus in children with autism. Mol Autism. 2014; 5:17. [PubMed: 24564936]

Uylings HBM, Malofeeva LI, Bogolepova IN, Jacobsen AM, Amunts K, Zilles K. No postnatal doubling of number of neurons in human Broca's areas (Brodmann areas 44 and 45)? A stereological study. Neuroscience. 2005; 136:715–28. [PubMed: 16344146]

Wegiel J, Kuchna I, Nowicki K, Imaki H, Wegiel J, Marchi E, Ma SY, Chauhan A, Chauhan V, Bobrowicz TW, de Leon M, Saint Louis LA, Cohen IL, London E, Brown WT, Wisniewski T. The neuropathology of autism: defects of neurogenesis and neuronal migration, and dysplastic changes. Acta Neuropathol. 2010; 119:755–70. [PubMed: 20198484]

Wegiel JJ, Flory M, Kuchna I, Nowicki K, Ma SY, Imaki H, Cohen IL, London E, Brown WT, Wisniewski T. Brain-region-specific alterations of the trajectories of neuronal volume growth throughout the lifespan in autism. Acta Neuropathol Commun. 2014; 2:28–46. [PubMed: 24612906]

West MJ, Slomianka L, Gundersen HJ. Unbiased stereological estimation of the total number of neurons in thesubdivisions of the rat hippocampus using the optical fractionator. Anat Rec. 1991; 231:482–97. [PubMed: 1793176]

West MJ, Slomianka L. Total number of neurons in the layers of the human entorhinal cortex. 1998; 82:69–82.

Yushkevich PA, Piven J, Hazlett HC, Smith RG, Ho S, Gee JC, Gerig G. User-guided 3D active contour segmentation of anatomical structures: significantly improved efficiency and reliability. Neuroimage. 2006; 31:1116–28. [PubMed: 16545965]

Zhao C, Deng W, Gage FH. Mechanisms and functional implications of adult neurogenesis. Cell. 2008; 132:645–60. [PubMed: 18295581]

Zilbovicius M, Meresse I, Chabane N, Brunelle F, Samson Y, Boddaert N. Autism, the superior temporal sulcus and social perception. Trends Neurosci. 2006; 29:359–366. [PubMed: 16806505]

Using stereological methods, the authors estimated that the isocortex of the human superior temporal gyrus contains approximately 91 million pyramidal neurons with an average somal volume of approximately 1500 μm^3. While neuron numbers were not correlated with age, pyramidal somal volume exhibited a significant linear decrease from childhood to adulthood.

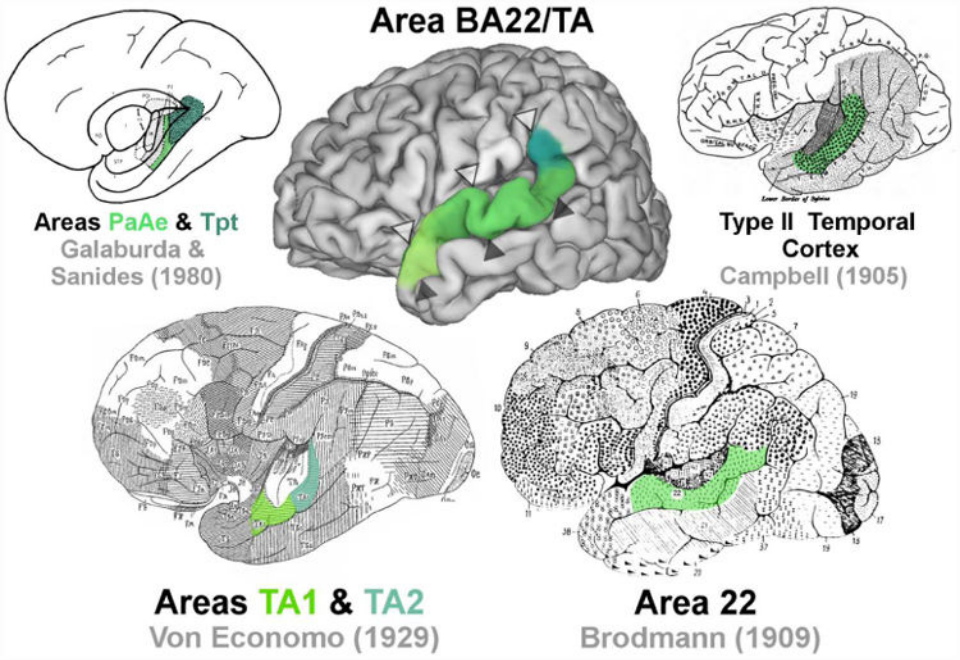

Figure 1.

A map of the approximate location of BA22/TA (middle) compared with classical maps of the region. Open arrowheads (Δ) indicate the position of the lateral sulcus. Closed arrowheads indicate the position of the superior temporal sulcus (STS) (▲).

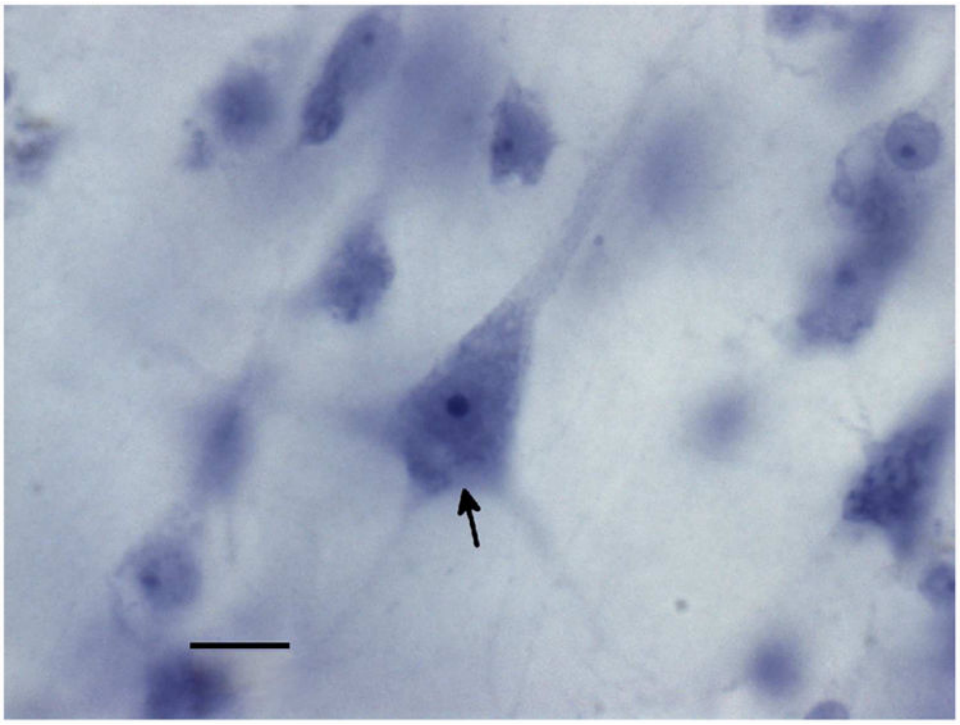

Figure 2.
Pyramidal neurons (arrow) were identified by their large size, triangular shape, and the presence of a pially oriented apical dendrite opposite one or more basilar dendrites. Scale bar represents 10 μms.

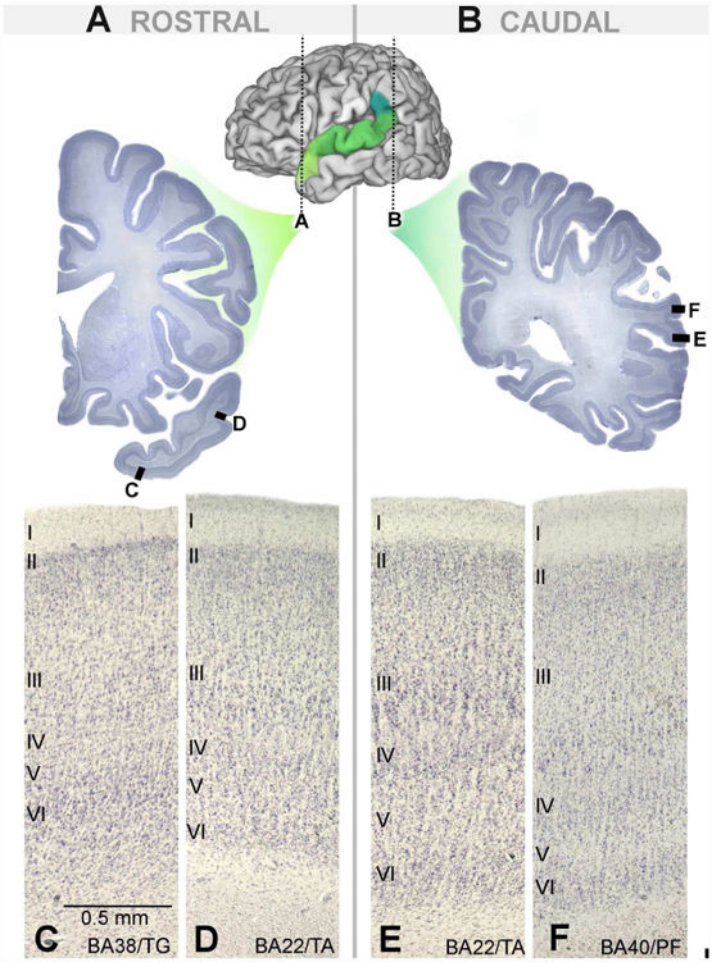

Figure 3.

Cytoarchitecture of BA22/TA and surrounding regions in rostral-most (A) and caudal-most sections (B). Area BA38/TG (C) forms the rostral boundary of anterior portions of BA22/TA (D). Posterior BA22/TA (E) is replaced by BA40/PF (F) in later sections.

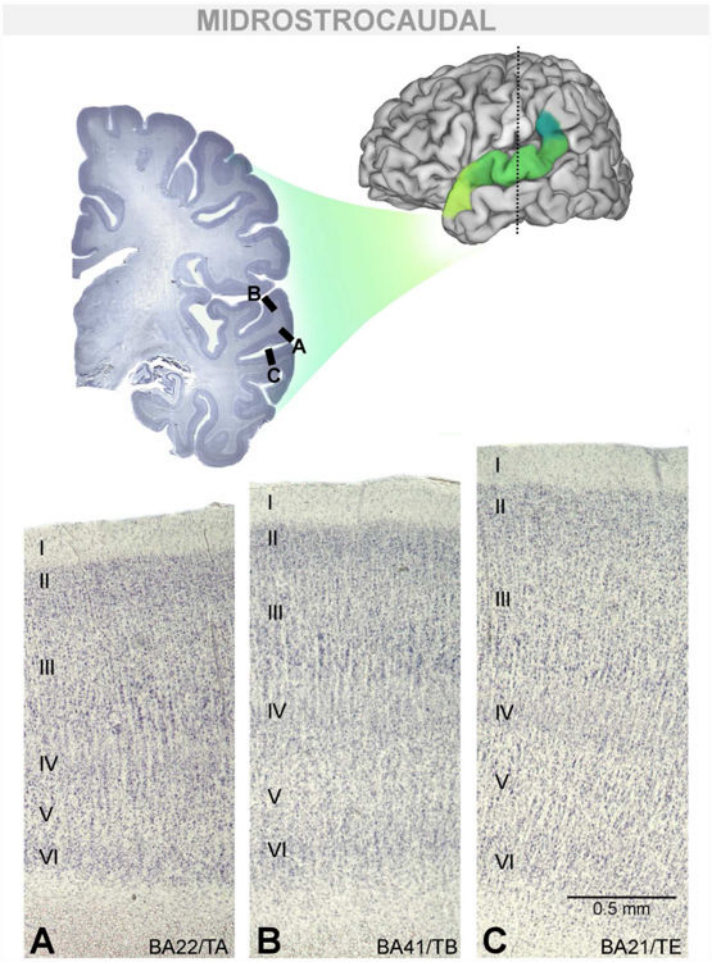

Figure 4.

Cytoarchitecture of BA22/TA and surrounding dorsomedial and ventromedial borders in a midrostrocaudal section. Midrostrocaudal BA22/TA (A) can be distinguished from BA41/TB (B), forming its dorsomedial border, and area BA21/TE (C), forming its ventromedial border.

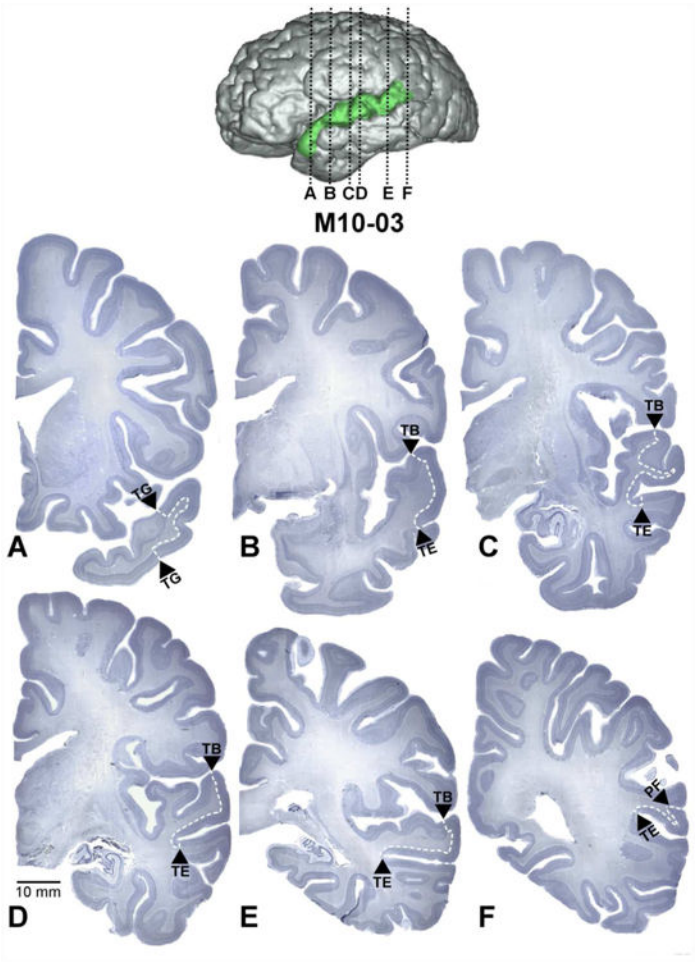

Figure 5.

Coronal sections demarcating the boundaries of BA22/TA through its rostrocaudal extent in case M10-03 (A-F). The approximate location of each section in the hemisphere is indicted by black dotted lines on a surface reconstruction of the same case. White dashed lines indicate the internal boundaries of BA22/TA. Arrowheads denote the name of the adjacent region sharing a border with BA22/TA at that level (Only von Economo's nomenclature is used for visual clarity). The scale bar represents 10 mm and applies to only to the coronal images. The distance between sections A and B is approximately 2.9 cm.

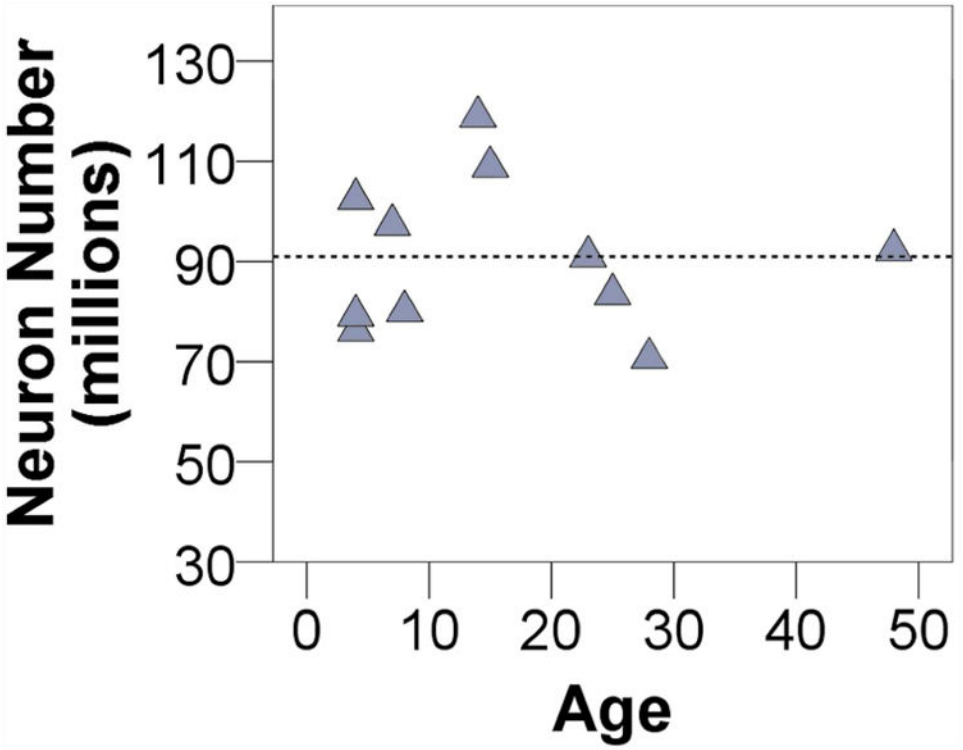

Figure 6.
Neuron number shows no association with age. The dashed line indicates the mean of the total sample.

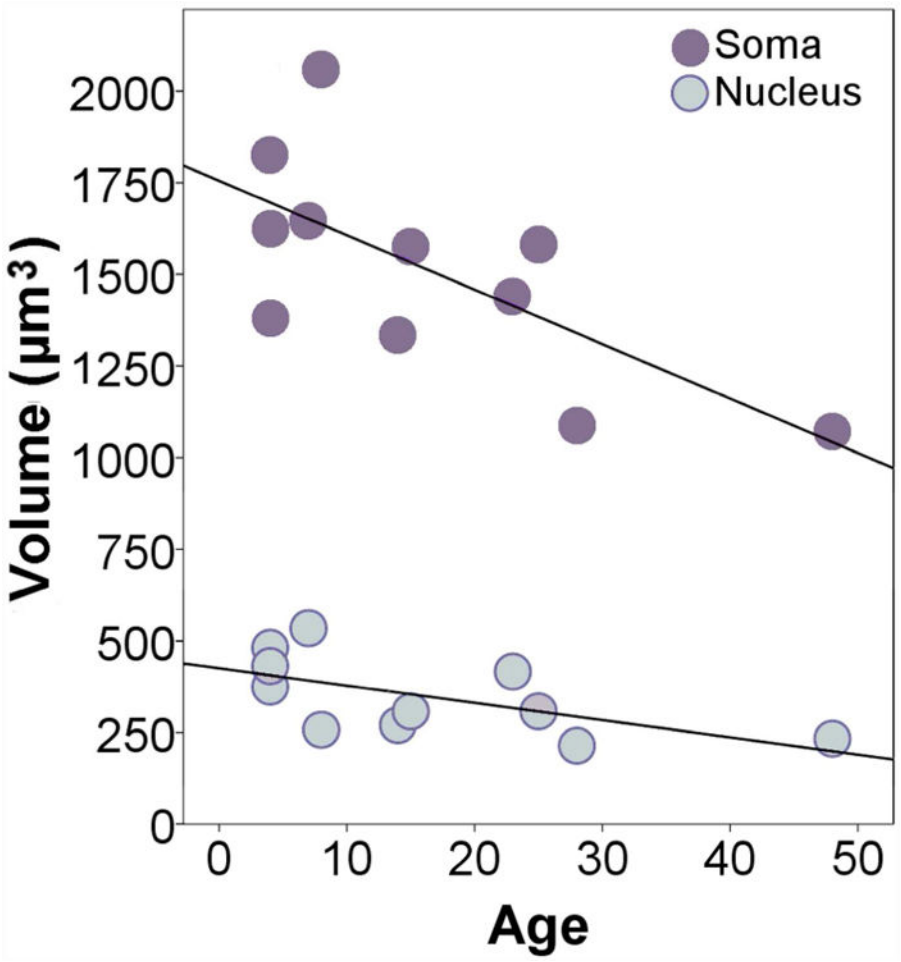

Figure 7.

Regression plot indicating a negative relationship between age and volume of pyramidal soma and nuclei. Somal volume: y = 1755.04 -14.85×, R^2 = 0.48, p = 0.02; Nuclear volume: y = 425.04 - 4.71×, R^2 = 0.37, p = 0.05.

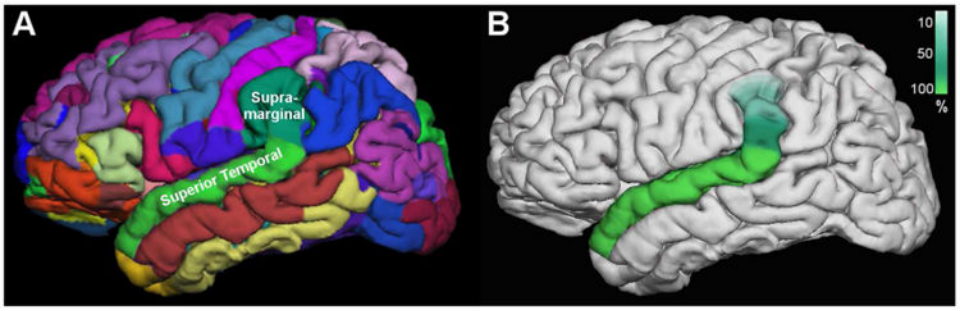

Figure 8.

Schematic comparing the automated parcellation scheme produced by FreeSurfer (A) with the approximate observed extent of the cytoarchitectural region in serial Nissl sections (B). The anterior boundary of the region on the superior temporal gyrus corresponds closely to sulcal maps, while the posterior boundary was more variable across cases and often extended beyond the superior temporal gyrus into the supramarginal gyrus. Variation in the height of the posterior region is summarized in B. The color scale indicates the percent of cases that exhibited a posterior boundary extending to the respective height in the hemisphere.

Table 1

Comparison of prior cytoarchitectonic descriptions of the isocortical region of the superior temporal gyrus

Superior Temporal Gyrus						
	Authors	**Layer II**	**Layer III**	**Layer IV**	**Layer V**	**Layer VI**
BA22/TA	Present Analysis	Relatively thin. Frayed border with layer I.	Thick. Dark medium to large sized pyramidals of IIIc overlay one another in columns creating a jagged appearance above layer IV.	Thin. Relatively cell sparse with less distinct borders. Columnar.	Coarse columnar appearance. Mainly medium pyramidals.	VIa cell dense with dark staining cells. Demarcation with WM not distinct.
TA (TA1/TA2)	von Economo, 1929	Relatively thin. Frayed border with layer I.	Rather thick. Contains uniformly medium-sized pyramidal cells so IIIc is hardly visible.	Relatively thin & sparse in cells. Columnar.	Medium sized pyramidal cells. Increased layer thickness rostrally (TA2). Cells smaller caudally (TA1).	Indistinct WM border. VIa cell dense. TA1 mostly triangular cells. TA2 mostly spindle shaped cells. TA2 has a less distinct radial orientation.
Type II Temporal Cortex	Campbell 1905	Less cell dense than in HG.	Significantly fewer “giant” cells, while having many more “large pyramidal” neurons than in HG.	Prominent band with radial oriented cells.	Reduced number of large pyramidals; less dense than adjacent temporal isocortex.	Fusiform cells fewer than in HG but more columnar.
Te3	Morosan et. al., 2005	Relatively broad.	IIIc cells prominent in size and density.	Relatively broad, especially compared to Te4/sulcal STG.	Denser inner pyramidal layer.	Cell dense and WM demarcation indistinct.
Rostral Subdivisions						
	Authors	**Layer II**	**Layer III**	**Layer IV**	**Layer V**	**Layer VI**
TAr	Ding et. al., 2009	Thicker and more densely packed than adjacent TG.	IIIa higher cell density with smaller pyramidal neurons. IIIb lower cell density with medium sized pyramidals.	Thick and prominent (relative to dysgranular TG).	Contains small to medium-sized pyramidal neurons.	Slightly higher cell density than layer V.
TAp	Ding et. al., 2009	Thicker and more densely packed with small round neurons than other portions of TA.	Loosely packed. Subdivided into IIIa (superficial) and IIIb (deeper) mainly consisting of medium to large sized pyramidals.	Thick and clear.	Small to med sized pyramidals arranged in small vertical columns.	Densely packed, mainly containing medium sized neurons. Not as columnar.
Area 22	Blaziot et. al., 2010	Distinct layer made up of small, stellate neurons.	Columnar organization of pyramidals.	Distinct thicker layer with columnar organization.	Well separated from layer VI. Columnar.	Not described.

Superior Temporal Gyrus						
	Authors	**Layer II**	**Layer III**	**Layer IV**	**Layer V**	**Layer VI**
Ts1e	Fullerton & Pandya, 2007	Irregular outer border; inner border blends with III.	Homogeneous with mainly small and some medium pyramidal cells.	Thin with a few small neurons.	Mainly small pyramidal neurons, layers not separable.	
Ts2i	Fullerton & Pandya, 2007	Outer border regular, inner border merges with III.	Upper layer contains small pyramidal cells. Lower contains a few medium pyramidal neurons.	Moderate in size.	Small and medium pyramidal cells, layers not separable.	
Ts2e	Fullerton & Pandya, 2007	Distinct outer border.	Upper contains small pyramidal neurons. Lower includes darkly-stained medium pyramidal.	More small cells than Ts1e.	Small-medium neurons; layers not separable.	
Caudal Subdivisions						
	Authors	**Layer II**	**Layer III**	**Layer IV**	**Layer V**	**Layer VI**
PaAe (External parakonio cortex)	Galaburda & Sanides 1980	Not described.	Medium sized pyramidals disposed in columns 3-8 cells deep in the deeper half of layer III.	Relatively narrow and less dense in cells.	Contains a large amount of pyramidal neurons.	Not described.
Tpt	Galaburda & Sanides 1980	Not described.	IIIc pyramidals offer an irregular border to IV in an undulating fashion.	Weaker than parakoniocortex & fuses with V.	More cell dense than parakoiniocortex.	Cell dense with branching columns of cells frequent.
Tpt	Sweet, et al. 2005	Not described.	Not described.	Fuses with III and V to create a broad band.	Not described.	Not described.
Ts3	Fullerton & Pandya, 2007	Denser than Ts2, inner border distinct.	Small and medium pyramidal cells with a few darkly-stained large pyramidal neurons.	Distinct and broader than Ts2.	Medium size neurons, layers not separable.	
PaAi	Fullerton & Pandya, 2007	Dense with distinct borders.	Upper contains small-medium neurons. Lower contains deeply-stained large pyramidal neurons.	Well developed and wide.	Small-medium pyramidal neurons.	Small-medium pyramidal neurons. Denser than V.
PaAe	Fullerton & Pandya, 2007	Broad layer.	Upper contains small-medium pyramidal neurons. Lower has darkly-stained large pyramidal.	Broader than PaAi.	Small-medium pyramidal neurons.	Small-medium pyramidal neurons. Slightly denser than V.
Tpt	Fullerton & Pandya, 2007	Broad, less dense than PaAe & PaAi	Upper contains small pyramidal cells. Lower has mostly medium, some large, pyramidal neurons.	Broad with irregular outer and inner margins.	Small-medium pyramidal neurons.	Small-medium pyramidal neurons. Layer VI distinct.

J Comp Neurol. Author manuscript; available in PMC 2016 May 01.

Abbr.: STG = superior temporal gyrus; HG = Heschl's gyrus; WM = white matter.

Table 2

Demographic characteristics of subjects in the analysis

Case	Age	Sex	Hemi	Cut Thickness (μms)	PMI (h)	Brain Weight (g)	Cause of Death
15-763-95	4	M	L	600	3	1,380	Heart Attack
426-02	4	F	R	200	21	1,222	Lymphocytic Myocarditis
M17-06	4	F	R	200	17	1,530	Acute Bronchopneumonia
15-138-97	7	F	L	500	74	1,350	Asthma
M3-04	8	F	R	200	20	1,222	Auto Accident
M9-03	14	M	R	200	20	1,464	Electrocution
M16-06	15	F	L	200	9	1,340	Auto Accident
444-02	23	M	R	200	6	1,520	Ruptured Spleen
9-1919-88	25	M	R	500	14	1,388	Cardiac Tamponade
M12-04	28	M	R	200	13	1,514	Multiple Injuries
M10-03	48	M	L	200	24	1,412	Arteriosclerosis

Abbr.: PMI = post mortem interval; Hemi = hemisphere.

Table 3

Stereological parameters for estimates of pyramidal neuron counts and volumes

Sampling Grid Area (μm²)		4,410,000
Counting Frame Area (μm²)		2,025
Disector Height (μm)		30
Guard Zone Height (μm)		10
Sections Sampled (Avg. #)		12
Mean Measured Thickness (μm)	*200 μm cut thickness*	179
	500 μm cut thickness	418
	600 μm cut thickness	550
Optical Fractionator Sample (Avg. #)		324
Optical Fractionator CE (Gundersen, M = 1)		< 0.07
Nucleator Sample (Avg. #)		81
Nucleator CE		<0.02

Mean measured thickness is presented for tissue that was originally sectioned at 200, 500, and 600 μms.

Table 4

Summary of cytoarchitectonic features that are most useful for distinguishing BA22/TA from each individual adjacent cortical territory

Features Distinguishing BA22/TA from Adjacent Areas				
	BA38/TG	**BA21/TE**	**B40/PF**	**BA41/TB**
General	In TA, columns are comparatively coarse, overall. Columns through the infragranular layers are often less distinct and less continuous with supragranular layers than in surrounding regions			
Layer II	TA is relatively thicker and more cell dense.	--	Boundary with III is more distinct in TA.	TA Thinner. Granule cells confined to layer II.
Layer III	Columns of dark staining cells in IIIc partially overlay one another, creating a jagged appearance above layer IV. IIIa and IIIb lighter, overall, with fewer dark cells.			
Layer IV	TA is relatively thicker and more cell dense.	Columnar and less distinct in TA	TA is columnar and more cell sparse.	TA is thinner. Granule cells confined to layer IV.
	Borders often blend into Layer III and V in TA			
Layer V	--	Often thinner in TA.	Tends to be wider in TA.	Darker and more cell dense in TA.
Layer VI	TA white matter transition gradual and indistinct.	Often thinner in TA. VIa is a distinct, darkly staining band in TA.	Tends to be wider in TA.	--

Table 5

Summary of stereological data

Case	Age	Sex	Pyramidal Neuron Number (×10^6)	Pyramidal Somal Volume (μm^3)	Pyramidal Nucleus Volume (μm^3)
15-763-95	4	M	76.27	1,624.48	481.36
426-02	4	F	102.48	1,827.00	431.25
M17-06	4	F	79.24	1,379.29	374.90
15-138-97	7	F	97.33	1,647.17	534.16
M3-04	8	F	80.11	2,060.21	257.58
Pre-Pubescent Average			**87.09 ± 11.93**	**1,707.63 ± 253.45**	**415.85 ± 106.36**
M9-03	14	M	118.89	1,335.06	270.04
M16-06	15	F	108.91	1,576.77	307.39
444-02	23	M	91.04	1,440.88	416.29
9-1919-88	25	M	83.48	1,582.47	307.64
M12-04	28	M	70.72	1,086.55	214.02
M10-03	48	M	92.30	1,071.87	233.14
Post-Pubescent Average			**94.22 ± 17.36**	**1,348.94 ± 228.35**	**291.42 ± 72.05**
Sample Average			**90.98 ± 14.88**	**1,511.98 ± 294.71**	**347.89 ± 106.50**

± standard deviation is included for averages.